

SPICE Simulation for Analysis and Design of Fast 1.55 μm MQW Laser Diodes

Giammarco Rossi, Roberto Paoletti, *Member, IEEE*, and Marina Meliga, *Member, IEEE*

Abstract—A rate equation model for static and dynamic behavior of 1.55 μm InGaAsP multi-quantum-well (MQW) semiconductor lasers has been developed. A three level scheme for the rate equations has been chosen in order to model carrier transport effects. The introduction of quasi-two-dimensional (quasi-2-D) gateway states between unbound and confined states has been used to calculate, for each well independently, carrier density and gain, allowing to take nonuniform injection into account. Starting from the formal identity between a rate equation and a Kirchoff current balance equation at a capacitor node, the model has been implemented on a SPICE circuit emulator. SPICE has granted an easy handling of parasitics and opens the possibility of integration with electrical components. The model's parameters have been directly derived from a complete set of measurements on real devices. Thanks to this characterization and the model accuracy, we have obtained good agreement between simulations and experimental data. The model was finally used to improve both static and dynamic properties of MQW devices. Based on this optimization, compressive strained InGaAsP/InP MQW Fabry–Perot lasers were realized, achieving low threshold current, high efficiency, and more than 10 GHz of direct modulation bandwidth.

Index Terms—Equivalent circuit, quantum-well lasers, semiconductor device measurement, semiconductor device modeling, semiconductor lasers.

I. INTRODUCTION

THE 1.55- μm InGaAsP/InP semiconductor laser diodes have been found to be key components in telecommunication networks, thanks to their speed and emission power [1]. With the advent of multi-quantum-well (MQW) structures, these characteristics have improved in terms of lower threshold current, higher internal efficiency and faster dynamics [1]. In the meantime, the development of lateral confinement structure based on semi-insulating materials (InP-doped with Fe or Co) [2]–[5] has allowed the strong reduction of parasitic capacitance and leakage currents, usually the limiting factors of the device performance.

However, the study of high-speed lasers has revealed small signal intensity modulation bandwidth far below the limit of the intrinsic material dynamics [6]. The origin of this behavior has been traced to carrier transport processes [6]–[11], namely, 1) *space transport*, drift-diffusion from the cladding across the optical confinement layer (OCL) [also called separate confinement heterostructure (SCH)] toward the active region

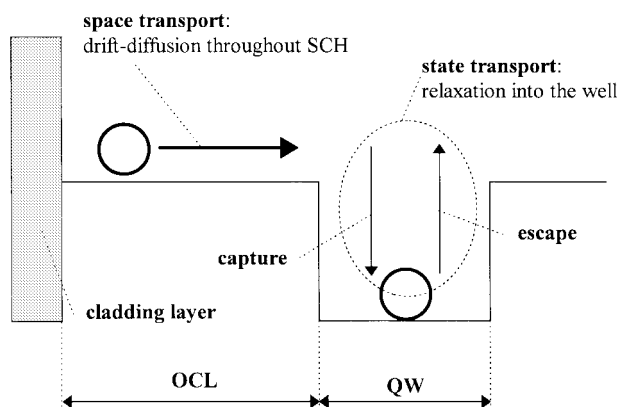


Fig. 1. Carrier transport processes in MQW layers.

and 2) *state transport*, relaxation of carriers at the bottom of the quantum well, net result of the competing phenomena of capture and escape (Fig. 1).

Starting from these considerations we have developed a model satisfying the requirements of fast computing and high accuracy. Rate equations have been chosen to avoid spatial derivatives and reduce the computational effort; always for sake of simplicity the ambipolar representation [7] of carrier population has been chosen. On the other side, we wanted a model able to deal with MQW structures preserving the discrete nature of QW's [10] and to distinguish between space and state transport [8]; so a three level representation of carrier energy states has been used [8], [12], which allows to treat each well independently from all the others. This is a strong point respect other equivalent circuit models of MQW structures [13], [14], where QW's are considered altogether, without any distinction between them.

A SPICE simulator was used [13] to solve the equations because it allows integration with electrical components (laser driver, package parasitic, etc.).

As far as we know, this is the first time that all the above elements have been included in a SPICE simulation program, supported by the accurate evaluation of the model parameters derived from device characterizations.

Based on the results obtained from the model, 1.55 μm InGaAsP strained MQW semi-insulating buried heterostructure (SI-BH) Fabry–Perot lasers have been realized. The active region was made of two 1.27 μm InGaAsP OCL layers (1000 Å), p doped ($5 \times 10^{17} \text{ cm}^{-3}$) on the p side, five InGaAsP 1% compressive strained wells (90 Å), and four 1.27 μm InGaAsP unstrained barriers (96 Å). Active region as well

Manuscript received June 23, 1997; revised January 12, 1998.

G. Rossi is with the University of Pavia, Pavia 27100 Italy.

R. Paoletti and M. Meliga are with Centro Studi E Laboratori Telecomunicazioni (CSELT) S.p.A., Torino 10148 Italy.

Publisher Item Identifier S 0733-8724(98)04824-5.

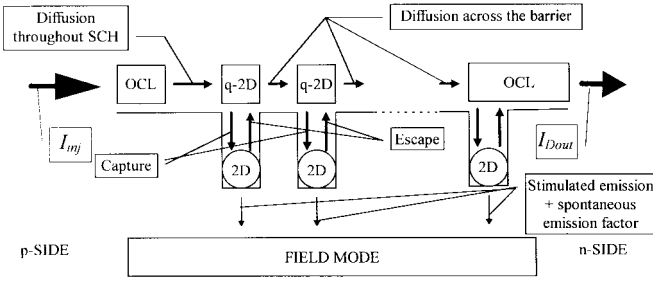


Fig. 2. Levels' scheme for rate equations. The quasi-2-D states act as gateways and allow to distinguish between state and space transport and to treat each well independently.

as Fe-doped SI blocking layers have been grown by MOCVD technique [3]. The devices have shown more than 10 GHz of modulation bandwidth, 7–12 mA of threshold current and 10 mW of optical power.

II. DESCRIPTION OF THE MODEL

We have represented the rate equations by means of a three level scheme, in order to model carrier transport effects, as shown in Fig. 2. Quasi-two-dimensional (quasi-2-D) states collect carriers in the well region with an energy higher than confined ones, hence their behavior is halfway between 2-D and three-dimensional (3-D) carriers. They act as gateway states between QW confined states and the bulk region of OCL; as it can be seen from Fig. 2, there are different quasi-2-D and 2-D states from well to well, therefore we can have a description of carrier distribution in every QW layer, recovering partially the information on spatial carrier profile lost with rate equations. Nonetheless quasi-2-D states can take into account space transport across OCL and barriers and state transport toward 2-D confined states, describing properly all transport processes.

The ambipolar model has been chosen [7]: under the condition of charge neutrality throughout the structure, the distinction between electrons and holes is eliminated, dealing simply with “carriers.” From a dynamic point of view, the ambipolar representation assumes that electrons are so faster than holes that they can reconfigure their distribution on a time scale much shorter than all the other processes. Even if in [9] it is reported that charge neutrality is not strictly respected in QW structures, we preferred to gather in terms of simplicity and computational speed, despite of a major accuracy.

A. Rate Equations and Gain Expression

From the model levels scheme reported in Fig. 2 we can deduce the rate equations. Carrier densities in different regions are distinguished by n with subscripts S , B , and W indicating, respectively, OCL, quasi-two-dimensional (2-D), and confined 2-D regions. A lowercase s stands for photon density.

The recombination of carriers in each of the regions listed above is expressed as [15], [16]

$$R_{S,B,W} = A_{S,B,W} n_{S,B,W} + B_{S,B,W} n_{S,B,W}^2 + C_{S,B,W} n_{S,B,W}^3 \quad (1)$$

where A , B , C are the well known recombination coefficients.

For the p-side OCL region, where we assume carriers are injected, we have the following expression:

$$\frac{dn_{S1}}{dt} = \frac{I_{inj}}{qV_{S1}} - R_{S1} - \frac{I_D}{qV_{S1}} \quad (2)$$

where V_{S1} is the OCL volume, I_{inj} is the injected current, and I_D the drift-diffusion current. We have described it by means of an effective space transport time [7] $\tau_D = L_S^2/2D_a$ [$D_a = D_n D_p / (D_n + D_p)$, ambipolar diffusivity] in the following way:

$$I_D = \frac{V_{S1} n_{S1} - V_W n_{B1}}{\tau_D} \quad (3)$$

where V_W is the well volume and n_{B1} the carrier density in the first well from p-side.

For the equation on the n-side we have included the quasi-2-D state of the last well (the first from n-side) in the OCL state. The result is

$$\begin{aligned} \frac{dn_{S2}}{dt} = & \frac{I_{D(N_{QW})} - I_{Dout}}{qV_S} - R_{S2} \\ & - \left[\frac{n_{S2}}{\tau_c} - \frac{V_W}{V_S} \frac{n_{W(N_{QW})}}{\tau_e} \right] \end{aligned} \quad (4)$$

where N_{QW} is the total number of wells. I_{Dout} has the following expression:

$$I_{Dout} = \frac{V_{S2} n_{S2}}{\tau_D} \quad (5)$$

The rate equations for the quasi-2-D states are given below

$$\frac{dn_{B(j)}}{dt} = \frac{I_{D(j)} - I_{D(j+1)}}{qV_W} - R_B - \left[\frac{n_{B(j)}}{\tau_c} - \frac{n_{W(j)}}{\tau_e} \right] \quad (6)$$

being τ_c and τ_e the carrier capture and escape times, and carrier densities in the j th quasi-2-D and 2-D state, respectively.

$I_{D(j)}$ for $j \neq 1$ represents the diffusion across the barrier between two adjacent wells and has the expression

$$I_{D(j)} = \frac{V_W n_{B(j)} - V_W n_{B(j-1)}}{\tau_B} \quad (7)$$

where $\tau_B = L_B^2/2D_a$ is the diffusion time across the barrier (L_B is the thickness of the barrier layer).

For $j = 1$ the current is the diffusion current of (3), for $j = N_{QW}$ (N_{QW} total number of wells) $n_{B(N_{QW})}$ does not exist because it has been included in n_{S2} , giving the current $I_{D(N_{QW})}$ of (4).

The equation for the confined states is given by

$$\frac{dn_{W(j)}}{dt} = \left[\frac{n_{B(j)}}{\tau_c} - \frac{n_{W(j)}}{\tau_e} \right] - R_{W(j)} - v_g G[n_{W(j)}, s] \quad (8)$$

where v_g is the group velocity and G is material gain which depends on the well carrier density and on the photon density.

Optical power is supposed to cause saturation by means of a gain suppression factor ε that reduces gain at high photon densities according to [7]–[9]

$$G[n_{W(j)}, s] = \frac{G[n_{W(j)}]}{1 + \varepsilon s} \quad (9)$$

Since $n_{W(j)}$ is the carrier density in the j th well, we can consider a different gain for each well depending upon its own carrier population.

For the expression of the carrier density dependent gain, we have chosen a logarithmic formula based on phenomenological considerations [17], [18]

$$G[n_{W(j)}] = G_O \left[1 + \ln \frac{n_{W(j)}}{N_O} \right]. \quad (10)$$

G_O and N_O are parameters extracted from characterization of real devices.

The photon density in the field mode is the result of the sum of the stimulated emissions from each well. Every single contribution is weighted by the optical confinement factor $\Gamma_{(j)}$, whose value is calculated for each well. It is also necessary to consider the coupling factor $\beta_{(j)}$ of spontaneous emission into the field mode [7]–[9]. We have made simulation using both different values of Γ for different wells and the same mean value for all the wells; valuable differences have been noted only in structures with a high number of wells, where Γ can vary significantly from one to another. The photon lifetime in the cavity τ_p is directly calculated from the measurement of the mirror reflection coefficient R_m and of the internal loss α , according to the formula [1], [17]

$$\tau_p^{-1} = [\alpha + \ln(R_m^{-1})/L_c]/v_g \quad (11)$$

where L_c is the cavity length. The result of such considerations is

$$\frac{ds}{dt} = \sum_{j=1}^k \Gamma_{(j)} v_g G[n_{W(j)}, s] s + \sum_{j=1}^k \Gamma_{(j)} \beta_{(j)} R_{sp}[n_{W(j)}] - \frac{s}{\tau_p} \quad (12)$$

where R_{sp} is the spontaneous emission rate which is approximated with the B coefficient of carrier lifetime (1) giving $R_{sp}[n_{W(j)}] = B n_{W(j)}^2$.

B. Leakage Effects and Handling of Parasitics

We have modeled two types of leakage effects, an electrical one, due to parasitic effects, and a heterojunction leakage.

The last one is a degradation of capture and escape ratio at high injection; the process is described in Fig. 3: since at higher current densities the mean energy of carriers is higher, the process of capture into the wells is less effective. This interpretation is supported by [8], where a dependence of capture and escape times on carrier temperature and concentration is reported.

To model this process, we have supposed that the ratio of capture time to escape time depends upon the current density according to the empirical formula

$$R = \frac{\tau_c}{\tau_e} = R_0 + R_1 J_{inj}^2. \quad (13)$$

Electrical leakage is easily accounted for by means of a nonlinear resistance; the chip parasitic behavior, including a parallel capacitor, is completely described by the equivalent circuit in Fig. 6. The active region injected current is the current flowing through the contact resistance.

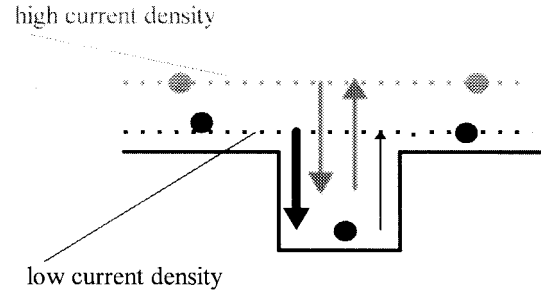


Fig. 3. Scheme of heterojunction leakage process: degradation of capture, escape time ratio. At higher injections the mean energy of carriers is higher (gray line) and so the capture process is less effective.

III. SPICE SIMULATION

Since, as reported in [13], [14], carriers density fluxes summing in a rate equation can be easily seen as a balance of currents at a capacitor node, the system of equations in Section II-A can be solved by means of a circuit simulator. So we have considered the idea of using SPICE to implement the model mainly for two reasons:

- 1) the possibility of integration with electrical components;
- 2) the fact that SPICE could avoid us to face the problems of writing the codes.

Hereafter, we report how the rate equations has been implemented on SPICE and the trick we had to use to make the simulator work properly (i.e., avoiding convergence problems and facing double solution equations).

A. Adapting Rate Equations to SPICE

Through a proper scaling, voltages are related to carrier densities, and currents to fluxes of particles or rates of exchange (i.e., capture, escape, or emission). This method avoids divergence in numerical simulations, while conserving a physical meaning of the variables.

Starting from (2), multiplying each equation by qV_{S1} gives us

$$V_{S1} \frac{d(qn_{S1})}{dt} = I_{inj} - I_{S1}^{ric} - I_D \quad (14)$$

where $I_{S1}^{ric} = qV_{S1}R_{S1}$ is the recombination current in the first OCL region.

Now, if we make the formal substitutions

$$\begin{aligned} v_{S1} &= qn_{S1} \\ C_{S1} &= V_{S1} \end{aligned} \quad (15)$$

we obtain the following equation for a capacitor node which can be described by the equivalent circuit of Fig. 4:

$$C_{S1} \frac{dv_{S1}}{dt} = I_{inj} - I_{S1}^{ric} - I_D. \quad (16)$$

In a similar way all the rate equations of Section II-A can be translated into equivalent circuits solvable by SPICE. The result for the entire active region is reported in the system of

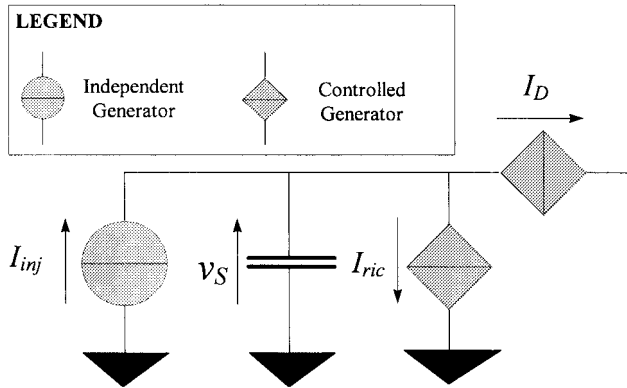


Fig. 4. Equivalent circuit of the optical confinement layer (OCL).

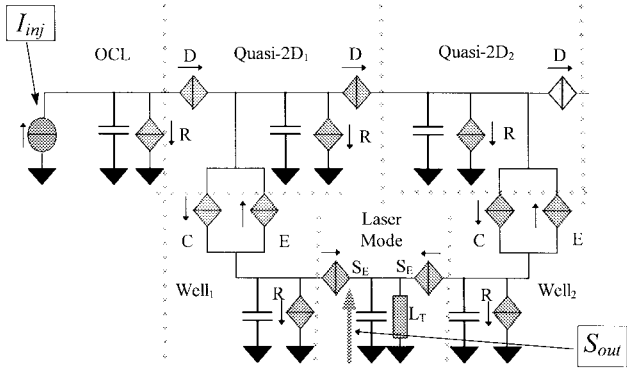


Fig. 5. Total equivalent circuit of quantum well active region. I_{inj} is the input injected current, while the output is the photon density S_{out} . Letters indicate the origin of dependent current generators: D stands for drift-diffusion [see (7)], R for recombination (13), C for capture, E for escape (19) and S_E for stimulated and spontaneous emission (21) and (22). L_T indicates photon lifetime equivalent resistance [see (23)].

equations below (equivalent circuit of Fig. 5)

$$C_B \frac{dv_{B(j)}}{dt} = [I_{D(j)} - I_{D(j+1)}] - I_{B(j)}^{ric} - [I_{C(j)} - I_{e(j)}] \quad (17)$$

$$C_{W(j)} \frac{dv_{W(j)}}{dt} = [I_{c(j)} - I_{e(j)}] - I_{W(j)}^{ric} - I_{stm(j)} \quad (18)$$

where as in (15) $I^{ric} = qVR$ is the recombination current, $v = qn$ and $C = V$; I_D is the diffusion current across the barrier and has the expression reported in (7).

Capture and escape currents are given by

$$I_c = qV_B \frac{n_B}{\tau_c}, \quad I_e = qV_W \frac{Rn_W}{\tau_c} \quad (19)$$

where R is the capture to escape time ratio.

The photon density was scaled by the photon energy $h\nu$. The equation for the field mode becomes then

$$C_{fm} \frac{dv_{fm}}{dt} = \sum_{j=1}^{N_{QW}} \Gamma_{(j)} I_{stm(j)} + \sum_{j=1}^{N_{QW}} \Gamma_{(j)} I_{sp(j)} - \frac{v_{fm}}{R_{fm}} \quad (20)$$

where

$$I_{stm(j)} = qV_W v_g G[(n_{W(j)}, s)]s \quad (21)$$

is the stimulated recombination current

$$I_{sp(j)} = qV_W \beta_{(j)} R_{sp}[n_{W(j)}] \quad (22)$$

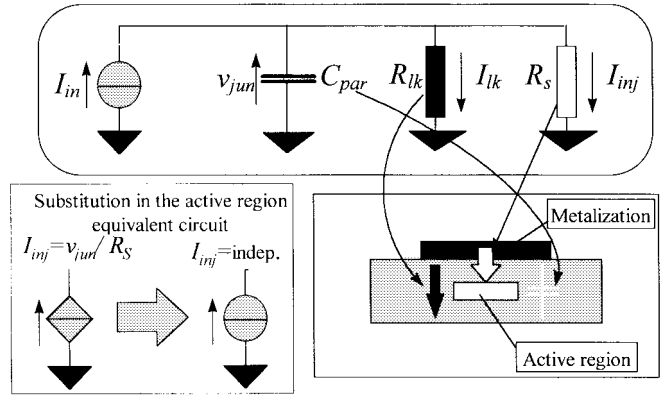


Fig. 6. Parasitic elements of the laser chip are taken into account through a parallel capacitor and a parallel leakage resistance.

the spontaneous emission current and finally

$$R_{fm} = \tau_p \frac{h\nu}{qV_W} \quad (23)$$

$$C_{fm} = \frac{qV_W}{h\nu} \quad (24)$$

are the photon lifetime equivalent resistance, accounting for internal and mirror losses, and the field mode equivalent capacitance.

B. Simulation of Static and Small-Signal Behavior

To simulate the static characteristic of a laser we had to face the problem of the double dc solution of (12): SPICE dc analysis was unable to resolve between the two. We have avoided the problem by running the simulation in transient mode giving as stimulus a linear ramp of current without a valuable penalty of calculation speed.

A similar problem has occurred calculating the bias point for the ac analysis; the way-out was to save the bias point while running the transient analysis and then to load it in the ac mode.

As an example of the model's simulation possibilities, Fig. 7 reports the Power-Current characteristic for different well numbers; in particular the simulation intends to show how heterojunction leakage affects different structures. In Fig. 8 it is described the nonuniform injection of carriers in a four QW structure, showing that wells next to p-side are more "filled" than the far ones, in agreement with [9]–[11], [19].

C. Large Signal Analysis and Photon Assisted Transport

The assumption of a discrete nature for quantum wells through the implementation of quasi-2-D states for each well and the large signal analysis mode of SPICE have allowed to model the photon assisted transport, a phenomenon related to nonuniform injection and reported for the first time by Eisenstein and Tessler [9], [11]. We can obtain similar results, compensating the minor accuracy with a considerable reduction of complexity and calculation speed (running the large signal analysis takes only a couple of minutes).

This process is typical of structures with a high number of wells: in case of step stimulus, the first wells fill faster,

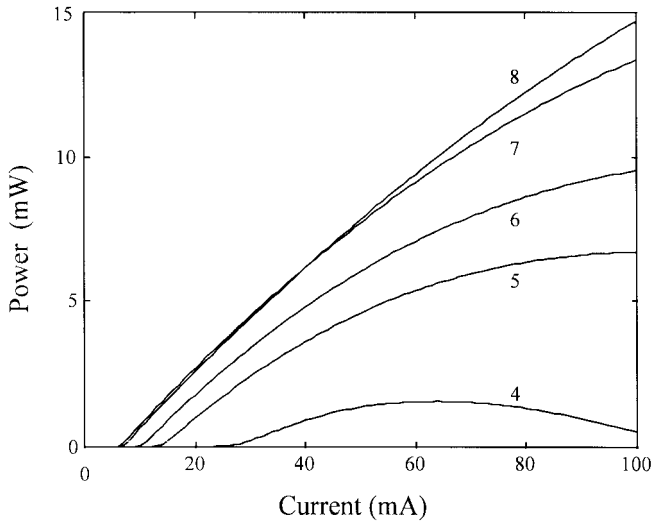


Fig. 7. Calculated *PI* characteristic obtained by varying the number of wells (from four to eight, for a device length of 200 μm) in presence of heterojunction leakage.

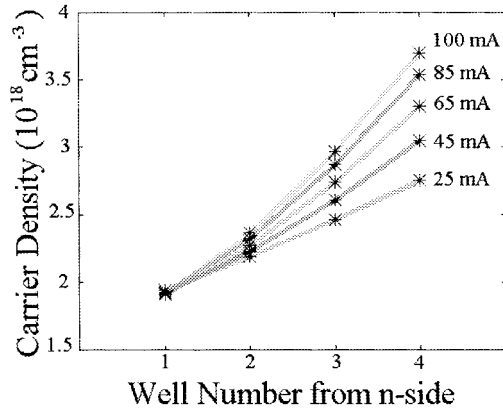


Fig. 8. Carrier injection nonuniformity in a four-QW laser at different bias points.

bringing the laser to threshold, the rapidly generated photons are then absorbed by the last well, causing a change in the slope of carrier concentration; this is simulated in Fig. 9 for a 15-well structure.

IV. COMPARISON WITH MEASUREMENTS

A. Extracting Model Parameters from Real Devices Characterization

The model presented till now grants reliability in terms of calculation speed and convergence problems, but in order to be reliable in its results, it needs a proper choice of the values of its parameters.

There are three categories of information needed:

- structural parameters: geometric dimensions, doping, etc.;
- chip parasitic values: parallel capacitance, series resistance;
- material characteristics: A , B , C recombination coefficients, internal loss, gain versus carrier density relation, carrier mobility.

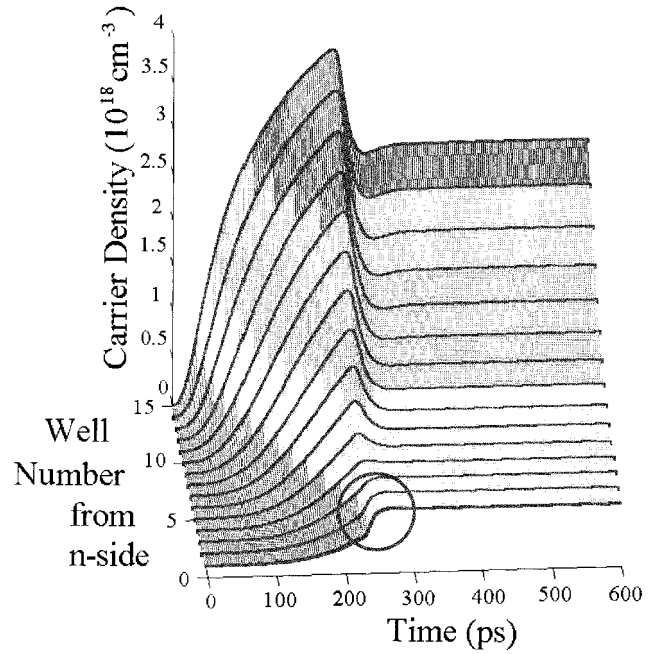


Fig. 9. Turn on transient in a 15 quantum well laser: in the circle the sudden rise of carrier concentration due to photon assisted transport can be easily seen.

Apart from the first category, all the other information can be obtained only by means of accurate characterization measurements. In order to compare the results of simulations and measurement, we must consider also static and dynamic behavior characterization.

In order to accomplish this task, we can rely on four types of measurements:

- 1) static PVI measurements, which give us optical power versus injection current characteristic, injection current versus junction voltage and differential series resistance;
- 2) dynamic characterization, involving small signal intensity modulation response and electrical reflection parameters (Smith Chart and parasitic capacitance) [20], [21];
- 3) gain measurement according to Hakki Paoli method, that estimates the internal losses and the material gain [22]–[24];
- 4) carrier lifetime measurement (carried out in a new way by means of optical modulation [25]) that gives us recombination rate versus carrier density (and so A , B , C coefficients through numeric interpolation) and carrier density as a function of injection current.

Combining data from 3) and 4) we can obtain gain as a function of carrier density and thereby extract the parameters G_O and N_O of (10). Since we have considered only five wells lasers, we have simply chosen the mean value to extract the single well gain; we are considering the possibility to grow single well structures to perform a more accurate evaluation of the parameters. By the way, we could verify that logarithmic gain fits well measurement as Fig. 10 clearly shows.

B. Comparison Between Simulations and Experiments

Measurement and parameters extraction as well as comparison between data and simulations have been made on

TABLE I

Name	Symbol	Process A	Process B	Derivation
Number of well		5	5	
Spontaneous emission factor	β	0.0001	0.0001	ref. [7]
Optical confinement factor (mean value for one well)	Γ	0.0235	0.0235	calculated
Trap aided recombination coefficient	A	$\sim 10^8 \text{ s}^{-1}$	$\sim 10^8 \text{ s}^{-1}$	measured
Radiative recombination coefficient	B	$\sim 10^{-11} \text{ s}^{-1} \text{ cm}^3$	$\sim 10^{-11} \text{ s}^{-1} \text{ cm}^3$	measured
Auger recombination coefficient	C	$\sim 10^{-28} \text{ s}^{-1} \text{ cm}^6$	$\sim 10^{-28} \text{ s}^{-1} \text{ cm}^6$	measured
Ambipolar Diffusivity	D_a	$\sim 1 \text{ s}^{-1} \text{ cm}^2$	$\sim 1 \text{ s}^{-1} \text{ cm}^2$	measured
Barrier width	L_B	9.6 nm	9.6 nm	measured
Well width	L_W	9 nm	9 nm	measured
Active region width	W	1.8 μm	2.3 μm	measured
Gain coefficient	G_O	950 cm^{-1}	980 cm^{-1}	measured
Gain carrier weighting coefficient	N_O	$2.5 \times 10^{18} \text{ cm}^{-3}$	$2.5 \times 10^{18} \text{ cm}^{-3}$	measured
Gain suppression factor	ε	5×10^{-17}	5×10^{-17}	ref. [7, 8]
Capture time	τ_c	1 ps	1 ps	ref. [8, 19]
Capture to escape time ratio (current independent ref. eq. (13))	R_0	0.01	0.01	ref. [8]
Capture to escape time ratio (current dependent ref. eq. (13))	R_1	$30 \times 10^{-12} (\text{cm}^2/\text{A})^2$	$30 \times 10^{-12} (\text{cm}^2/\text{A})^2$	ref. [8]
Internal losses	α	40 cm^{-1}	30 cm^{-1}	measured
Facet reflectivity	R_m	0.32	0.32	measured
Parasitic capacitance	C_p	6.5 pF	7 pF	measured
Parasitic series resistance	R_p	4 Ω	3.5 Ω	measured

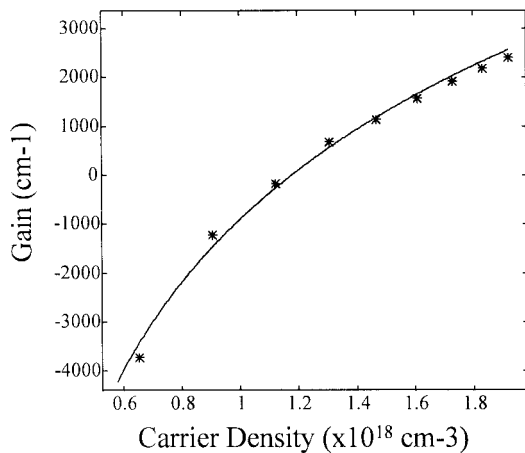


Fig. 10. Gain versus carrier density characteristic of a MQW laser device extracted from Hakki-Paoli and carrier lifetime measurement: measure data (asterisks) are well fitted by a logarithmic relation (continuous line). Measurement refers to the structures described in Section IV-B, Process A. Since it is a five-well structure, the values reported above give the mean value for the single well.

1.55 μm InGaAsP strained MQW Semi-Insulating Buried Heterostructure (SI-BH) Fabry-Perot lasers. The active region was made of two 1.27 μm InGaAsP OCL layers (1000 \AA), p-doped ($5 \times 10^{17} \text{ cm}^{-3}$) on the p-side, five InGaAsP 1% compressive strained wells (90 \AA), and four 1.27 μm InGaAsP unstrained barriers (96 \AA). We have first fabricated a process with a 1.8- μm wide active stripe (Process A) and, after its analysis by means of the simulator, a second process with a 2.3- μm wide active stripe (Process B). The related values of the model parameters are summarized in Table I.

The accuracy of the parameter measurements and the proper modeling of the phenomena involved, have given simulation results in good agreement with experimental data, for both static and dynamic characteristics.

In Figs. 11 and 13 the static PI characteristic of the different lasers is reported, showing a correct simulation even at high injection rate. Figs. 12 and 14 illustrate the small signal intensity modulation response: the agreement between calculations and experiments is extremely good.

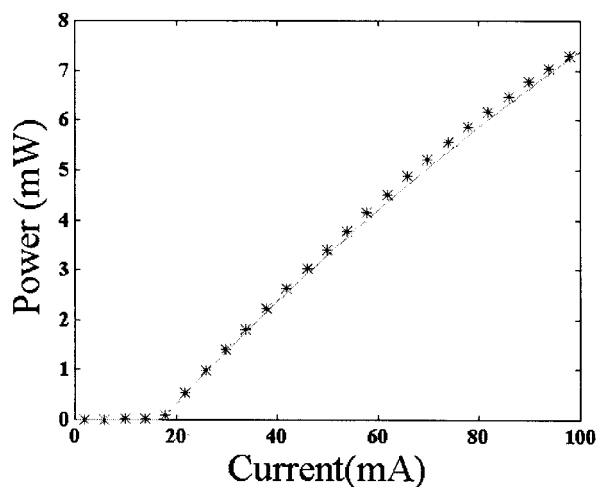


Fig. 11. Static characteristic for a 400- μm long device at 20 °C (Process A). Asterisks stands for data and continuous line for simulation.

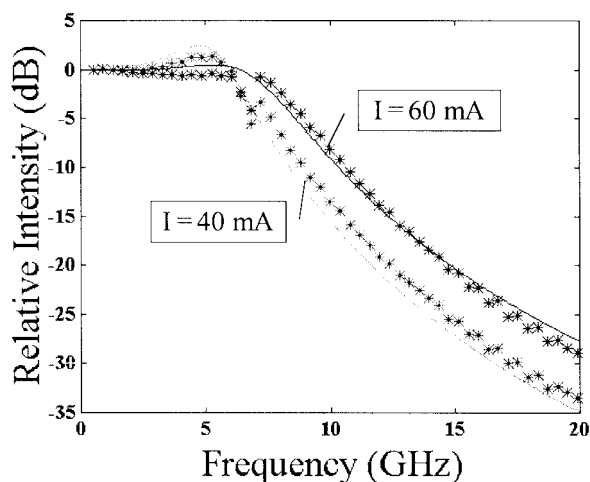


Fig. 12. Small signal intensity modulation response for a 400- μm long device at 20 °C (Process A) at two different bias currents (* data,—simulation). The notch at 7 GHz is due to wire bonding parasitic inductance and it is not included in the model.

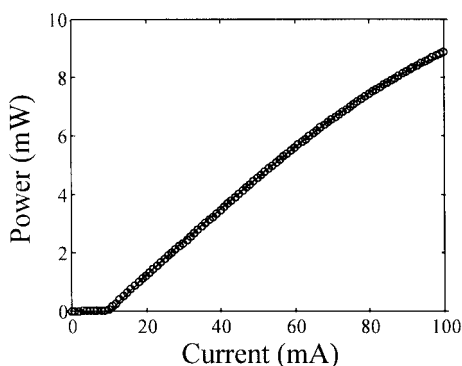


Fig. 13. Measurement (o) and simulation (-) of Power-Current characteristic in a wider stripe, 400 μm long device at 20 °C (Process B). Wider stripes reduce current density and so make heterojunction leakage less effective.

C. Improvement of Device Performance

In our intention this simulator should perform two tasks:

- 1) to analyze the device behavior, defining the main limitations in both static and dynamic characteristics;

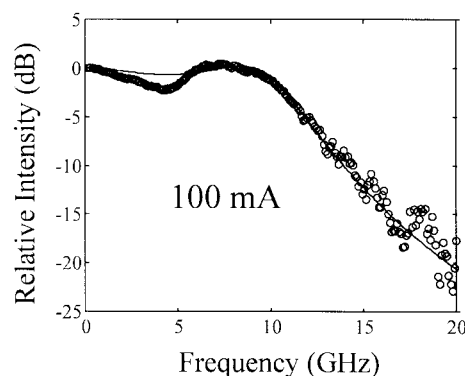


Fig. 14. Measurement (o) and simulation (-) of the improved bandwidth of a wider stripe, 400 μm long device (Process B). The measure, made at 100 mA 20 °C, shows a bandwidth of 11 GHz.

- 2) to foresee the effects of changes in the laser structure in order to improve its performance.

Actually this has been obtained on Process A in the case of *PI* saturation at high injection. We have supposed this behavior be mainly due to heterojunction leakage effects [1], that is related to the high current densities, as stated in Section II-B. Simulations have revealed that a wider active stripe could reduce this drawback.

Our assumptions have been validated by the analysis of Process B, obtained from the same material, but with larger active region. In these devices we have achieved an improvement of the *P-I* curve linearity, and a wider small signal bandwidth (Figs. 13 and 14).

V. CONCLUSIONS

A three level rate equation model has been implemented on a SPICE simulator. By means of a gateway quasi-2-D state placed in the well region, the model can treat each well independently and hence evaluate spatial diffusion, nonuniform current injection into different wells and consequently to calculate, for each quantum well, carrier population and carrier dependent gain.

The equations have been implemented on a SPICE circuit emulator, since a rate equation is formally analogue to a current balance at a capacitor node. SPICE grants easy handling of parasitic contributions and integration with electrical circuit components.

Since the accuracy of the results depends strongly on the model's parameters, a set of measurements has been performed to extract their values for real devices. Simulations have hence shown good agreement with measured static and dynamic characteristics.

The model has been used to inspect the behavior of devices and to find out possibilities of performance improvement.

Using the model, new devices have been made, showing lower threshold current, higher quantum efficiency and wider small signal bandwidth.

ACKNOWLEDGMENT

The authors would like to thank Prof. S. Donati of the University of Pavia, Italy, for his help and support, D. Bertone of CSELT, who fabricated the MQW structures, G. Magnetti,

G. Morello, and R. Y. Fang of CSELT for laser processing and realization, V. Guja of Politecnico di Torino, Italy, and P. Rosso for their help in characterizing laser devices.

REFERENCES

- [1] Y. Suematsu and A. R. Adams, *Handbook of Semiconductor Laser and Photonic Integrated Circuits*. London, U.K.: Chapman & Hall, 1994, pp. 1–22.
- [2] W. H. Cheng, S. Y. Huang, A. Appelbaum, J. Pooladdej, *et al.*, "Wide-band modulation of 1.3 μm InGaAsP buried crescent lasers with iron and cobalt-doped semi-insulating current blocking layers," *IEEE J. Quantum Electron.*, vol. 25, pp. 1353–1361, June 1989.
- [3] D. Bertone, A. Bricconi, R. Y. Fang, L. Greborio, G. Magnetti, M. Meliga, and R. Paoletti, "MOCVD regrowth of semi-insulating InP and p-n junction blocking layers around laser active stripes," *J. Crystal Growth*, vol. 170, pp. 715–718, 1997.
- [4] R. Y. Fang, D. Bertone, A. Bricconi, L. Greborio, G. Magnetti, M. Meliga, G. Morello, and R. Paoletti, "A new technological process to realize InGaAsP/InP semiinsulating buried heterostructure lasers emitting at 1.55 μm ," in *Proc. ESSDERC'96*, Bologna, Italy, Sept. 9–11, 1996, Session D5, pp. 533–536.
- [5] R. Paoletti, D. Bertone, A. Bricconi, R. Y. Fang, L. Greborio, G. Magnetti, and M. Meliga, "Comparison of optical and electrical modulation bandwidths in three different 1.55 μm InGaAsP buried laser structures," in *Photon. West 96, Functional Photon. Fiber Devices*, San Jose, CA, Jan. 30–Feb. 1, 1996, vol. 2695, pp. 296–305.
- [6] R. Nagarajan, T. Fukushima, M. Ishikawa, J. E. Bowers, R. S. Geels, and L. A. Coldren, "Transport limit in high-speed quantum-well lasers: Experiment and theory," *IEEE Photon. Technol. Lett.*, vol. 4, pp. 121–123, Feb. 1992.
- [7] R. Nagarajan, T. Fukushima, M. Ishikawa, J. E. Bowers, and R. S. Geels, "High speed quantum well lasers and carrier transport effects," *IEEE J. Quantum Electron.*, vol. 28, pp. 1990–2008, Oct. 1992.
- [8] C. Y. Tsai, C. Y. Tsai, Y. H. Lo, R. M. Spencer, and L. F. Eastman, "Nonlinear gain coefficients in semiconductor quantum-well lasers: Effects of carrier diffusion, capture and escape," *IEEE J. Select. Topics Quantum Electron.*, vol. 1, pp. 316–329, June 1995.
- [9] N. Tessler and G. Eisenstein, "On carrier injection and gain dynamics in quantum well lasers," *IEEE J. Quantum Electron.*, vol. 29, pp. 1586–1595, Nov. 1995.
- [10] ———, "Distributed nature of quantum-well lasers," *Appl. Phys. Lett.*, vol. 62, no. 1, pp. 10–12, Jan. 1993.
- [11] ———, "Transient carrier dynamics and photon-assisted transport in multiple-quantum-well lasers," *IEEE Photon. Technol. Lett.*, vol. 5, pp. 291–293, Mar. 1993.
- [12] D. McDonald and R. F. O'Dowd, "Comparison of two- and three-level rate equations in the modeling of quantum-well lasers," *IEEE J. Quantum Electron.*, vol. 31, no. 11, pp. 1927–1934, Nov. 1995.
- [13] M. F. Lu, C. Juang, M. J. Jou, and B. J. Lee, "Equivalent circuit of quantum well lasers," *IEEE J. Quantum Electron.*, vol. 31, pp. 1418–1422, Aug. 1995.
- [14] ———, "Study of carrier transport effects on quantum well lasers using a SPICE simulator," *Inst. Elect. Eng. Proc.—Optoelecton.*, vol. 142, no. 5, pp. 237–240, Oct. 1995.
- [15] W. C. Rideout, J. LaCourse, and R. B. Lauer, "Radiative and nonradiative recombination mechanism in 1.5 μm MQW lasers," in *12th IEEE Semiconduct. Laser Conf.*, Davos, Switzerland, Sept. 9–14, 1990, pp. 86–87.
- [16] R. Olshansky, C. B. Su, J. Manning, and E. W. Powazinik, "Measurement of radiative and non radiative recombination rates in InGaAsP and AlGaAs light sources," *IEEE J. Quantum Electron.*, vol. QE-20, pp. 838–854, Aug. 1984.
- [17] L. A. Coldren and S. W. Corzine, *Diode Lasers and Photonic Integrated Circuits*. New York: Wiley, 1995, pp. 44–45.
- [18] T. A. DeTemple and C. M. Herzinger, "On the semiconductor laser logarithmic gain-current density relation," *IEEE J. Quantum Electron.*, vol. 29, pp. 1246–1252, May 1993.

- [19] H. Hirayama, J. Yoshida, Y. Miyake, and M. Asada, "Carrier capture time and its effect on the efficiency of quantum well lasers," *IEEE J. Quantum Electron.*, vol. 30, pp. 1246–1252, Jan. 1994.
- [20] R. S. Tucker and D. J. Pope, "Microwave circuit models of semiconductor injection lasers," *IEEE Trans. Microwave Theory Tech.*, vol. MTT-31, pp. 289–294, Mar. 1983.
- [21] F. Delpiano, R. Paoletti, P. Audagnotto, and M. Puleo, "High frequency characterization of high performance DFB laser modules," *IEEE Trans. Comp., Packag., Manufact. Technol.*, vol. 17, pp. 412–417, Aug. 1994.
- [22] B. W. Hakki and T. L. Paoli, "I. cw degradation at 300 °K of GaAs double-heterostructure junction lasers. II. Electronic gain," *J. Appl. Phys.*, vol. 44, no. 9, pp. 4113–4119, 1973.
- [23] ———, "Gain spectra in GaAs double-heterostructure injection lasers," *J. Appl. Phys.*, vol. 46, no. 3, pp. 1299–1306, 1975.
- [24] P. A. Morton, D. A. Ackerman, G. E. Shtengel, R. F. Kazarinov, M. S. Hybertsen, T. Tanbun-Ek, R. A. Logan, and A. M. Sergent, "Gain characteristics of 1.55- μm high-speed multiple-quantum-well lasers," *IEEE Photon. Technol. Lett.*, vol. 7, pp. 833–835, Aug. 1995.
- [25] R. Paoletti, M. Meliga, and I. Montrosset, "Optical modulation technique for carrier lifetime measurement in semiconductor lasers," *IEEE Photon. Technol. Lett.*, vol. 8, pp. 1447–1449, Nov. 1996.



Giammarco Rossi was born in Castel San Giovanni (Piacenza), Italy, in 1970 and received the Laurea degree in electronics engineering at the University of Pavia, Italy, in 1994 with a thesis on quantum effects in photodetection. He is currently pursuing the Ph.D. degree in electronics engineering and computer science at the University of Pavia, working in the Optoelectronics Group and with the Optoelectronic Devices Unit of Centro Studi E Laboratori Telecomunicazioni (CSELT), Torino.

His main research interests are simulation and characterization of laser devices for fast communication systems.



Roberto Paoletti (M'96) was born in Vado Ligure (Savona), Italy, in 1966. He received the Laurea degree in electronic engineering from the University of Genova, Italy, in 1991 and the Ph.D. degree in electronics at the Electronic Department of Politecnico of Turin, Italy, in 1995.

In 1995, he joined the Centro Studi E Laboratori Telecomunicazioni (CSELT), Torino, Italy. In the last few years, he has been involved in research on characterization and design of high-speed optoelectronic devices.



Marina Meliga (M'95) was born in Cengio, Italy, on December 20, 1956. She received the Laurea degree in physics from the University of Torino, Italy, in 1981, where she worked on solar cells. Since 1984, she was with CSELT, Torino, Italy, where she worked on thin-film technology and laser design, modeling and characterization.

In 1992, she assumed the responsibility of the Optoelectronic Devices Unit in the Optical Systems and Technology Department of CSELT. She is author and coauthor of more than 50 papers on thin-film deposition and measurement techniques for integrated optics and laser design and characterization.